Unsteady pressure measurements on a 5:1 rectangular cylinder

Unsteady pressure measurements on a 5:1 rectangular cylinder

A.J. Bronkhorst [a,b], C.P.W. Geurts [a,b], C.A. van Bentum [a]

[a] *TNO, Built Environment and Geosciences, Delft, the Netherlands*
[b] *Eindhoven University of Technology, Department of Architecture, Building and Planning, Eindhoven, the Netherlands, a.j.bronkhorst@tue.nl*

1 INTRODUCTION

The "Benchmark on the Aerodynamics of a Rectangular Cylinder" (BARC) is an excellent opportunity for international collaboration of experimental and computational researchers to advance the research in high-Reynolds number bluff body aerodynamics. This paper will contribute to the BARC through the experimental analysis of the pressures on a 5:1 rectangular cylinder in a low-turbulence flow. The simplified conditions such as quasi two-dimensional flow and homogeneous turbulence, allow for a better understanding of the underlying mechanisms responsible for the pressures and loads encountered on bluff bodies such as buildings or bridges.

In the 1980s such experiments on velocity and pressure were performed by e.g. Hillier and Cherry (1981) and Kiya and Sasaki (1983). The goal of these studies was to obtain more knowledge of the mean and fluctuating effects of flow separation and reattachment on a long flat plate. The studies showed that an increase in free stream turbulence produces a significant contraction of the separation bubble and increases the mean suction and the intensity of pressure fluctuations caused by this separation bubble. The peak in fluctuating pressures occurs somewhat upstream of mean re-attachment (Hillier and Cherry, 1981); it is caused by two agents: the motion of the large-scale vortices; and the low-frequency unsteadiness [see Kiya and Sasaki (1985) for a detailed explanation]. Saathoff and Melbourne (1989) found similar results for mean and standard deviation pressure coefficients on a flat plate; they also investigated the measured peak pressure coefficients in the separation and reattachment zone. In a low turbulent flow the peak pressure coefficients near the leading edge do not deviate significantly from the mean pressure coefficients. The peak pressure coefficients become larger moving downstream along the plate, due to an increase in pressure fluctuation intensity. At the point where mean pressure recovery (i.e. the region on the plate where the mean pressure has an adverse gradient) starts, the peak pressure coefficient distribution shows its largest value ($C_{p,min} \approx -1.1$).

Surry and Djakovich (1995) explored extreme peak suctions, sometimes encountered on high-rise building models, and their relationship with building shape and oncoming simulated atmospheric flow characteristics. With findings described in earlier fundamental research [e.g. Hillier and Cherry (1981) and Saathoff and Melbourne (1989)] they determined some of the underlying flow mechanisms responsible for peak pressures in a more complex environment. Although they did not present extreme peak suctions, there study provided a better understanding of the relation between peak suctions and the flow mechanisms encountered around buildings.

This paper discusses the results of measurements performed on a 5:1 rectangular cylinder. Results and knowledge obtained in this study will be used to better describe pressure effects encountered on building models in an urban environment.

2 DESCRIPTION WIND TUNNEL EXPERIMENT

Measurements on a 5:1 rectangular cylinder were performed in an open circuit Boundary Layer wind tunnel. Near the air inlet four anti-turbulence grids reduce the turbulence created by the intake. The working section has a length of approximately 13.5 m; the test section has a width of

3 m, a height of 2 m and a length of 11 m. For this quasi two-dimensional experiment no roughness devices were placed in the working section.
The oncoming flow was measured above the centre of the turntable with a one-component Dantec Dynamics hot wire anemometer. Ten measurements were performed with a 500 Hz sampling frequency for a total period of approximately 41 s. At a Reynolds number of 0.5 x 10^5 the velocity was 7.51 (+/- 0.2) m/s and the longitudinal turbulence intensity was 0.44 (+/- 0.12). At a Reynolds number of 1.0 x 10^5 the velocity was 15.16 (+/- 0.04) m/s and the turbulence intensity was 0.38 (+/- 0.05).

The wind tunnel model, illustrated in Figure 1, has a cross section of 0.5 m x 0.1 m (B x D) and a total length L = 2 m, resulting in a blockage ratio of $A_{fr.,\,model} / A_{fr.\,wt}$ x 100% ≈ 3.5% at $\alpha = 0^o$. The model consists of plastic and wooden parts. To investigate the influence of edge sharpness on the measured pressures, interchangeable elements with radii of curvature of R/D = 0, 0.01, 0.02 and 0.5 were constructed for the corners. A metal frame supporting the model over its height provides for enough stiffness to prevent dynamic effects. A plastic plate taped at the ceiling of the wind tunnel provided support at this end, a hinge (Figure 1) inside the model allowed the model to rotate with the turn table. As the flow field is very sensitive to the orientation of the cylinder (Robertson et al, 1977), alignment and angle of incidence of the model need to be determined as accurately as possible. The model axes were aligned with the wind tunnel axes within 0.5 mm accuracy. The large radius of the turn table, r = 1.15 m, allows for an angle setting with an accuracy of approximately 0.05 degree. The zero degree angle of incidence was obtained with a similar accuracy through alignment with one of the wind tunnel side walls.
The model was instrumented with 88 pressure taps, as illustrated in Figure 2. The pressure tubes in the model surface have an internal diameter of 1.1 mm. The pressure tubes were linked to three 32-channel analog pressure scanning module (ZOC23B). These modules are simultaneously sampled by a Scanivalve Digital Service Module (DSM) 3400 for approximately 120 s at 400 Hz.
During pressure measurements a pitot-static tube was used to determine the approach-flow velocity and the dynamic pressure. It is located at the height of the instrumented section, approximately 2.6 m ahead of the models centre, and 0.7 m to the side.
The basic measurement, required by the BARC specifications (Bartoli et al, 2008), was performed at a velocity of 7.5 m/s yielding a Reynolds number $Re = UD/v$ of 0.5 x 10^5. Additional sensitivity measurements were planned on the Reynolds number (Re = 1.0 x 10^5), the angle of incidence (α = 0.5º, 1º, 3º, 6º and 15º) and the edge sharpness (R/D = 0, 0.01, 0.02 and 0.05).

The measured pressures are converted into mean and standard deviation pressure coefficients using:

$$C_{\bar{p}} = \frac{\bar{p}}{\frac{1}{2}\rho U_{ref}^2} \quad \text{and} \quad C_{\sigma_p} = \frac{\sigma_p}{\frac{1}{2}\rho U_{ref}^2}. \tag{1}$$

In which $\bar{p}$ and σ_p are the mean and standard deviation of the measured pressure signal.
For the analysis of the extreme values, the sample record is divided in intervals with a non-dimensional time tU/D = 50. For each interval the measured pressures are converted to maximum and minimum pressure coefficients with:

$$C_{\hat{p}} = \frac{\hat{p}}{\frac{1}{2}\rho U_{ref}^2} \quad \text{and} \quad C_{\check{p}} = \frac{\check{p}}{\frac{1}{2}\rho U_{ref}^2}. \tag{2}$$

In which $\hat{p}$ and $\check{p}$ are the maximum and minimum pressure of an interval. A peak pressure coefficient is obtained by determining the mean of all maxima and minima. The resulting peak provides a more reliable value than the single measured extreme from the complete sample record.

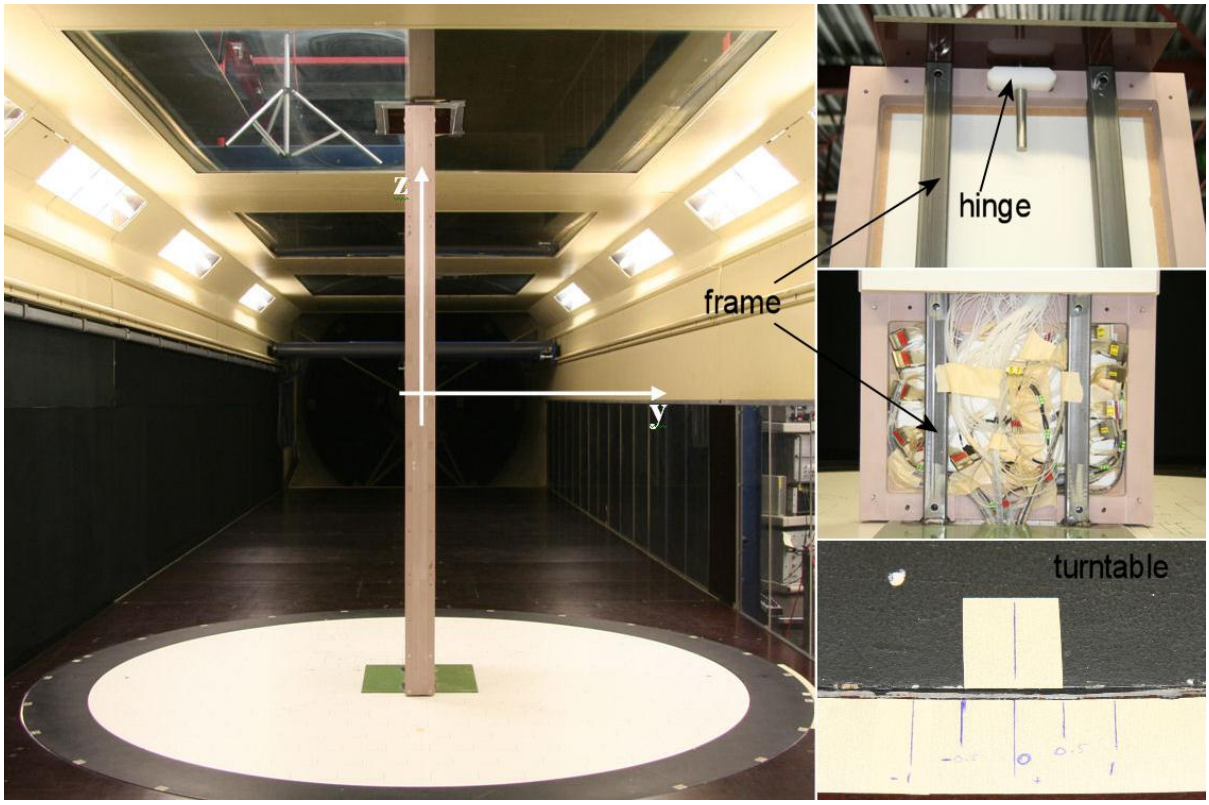

Figure 1. Illustration of the model positioned on the turn table in the wind tunnel. The reference system is located at the centre of the wind tunnel model, 1 m above the centre of the turn table. The top detail illustrates the hinge inside the model and the plate connecting this end of the model to the glass wind tunnel wall. The middle detail shows the supporting frame at the bottom of the model, the steel bars extend throughout the height of the model. The bottom detail illustrates the use of the turn table to define the angle setting with a higher accuracy.

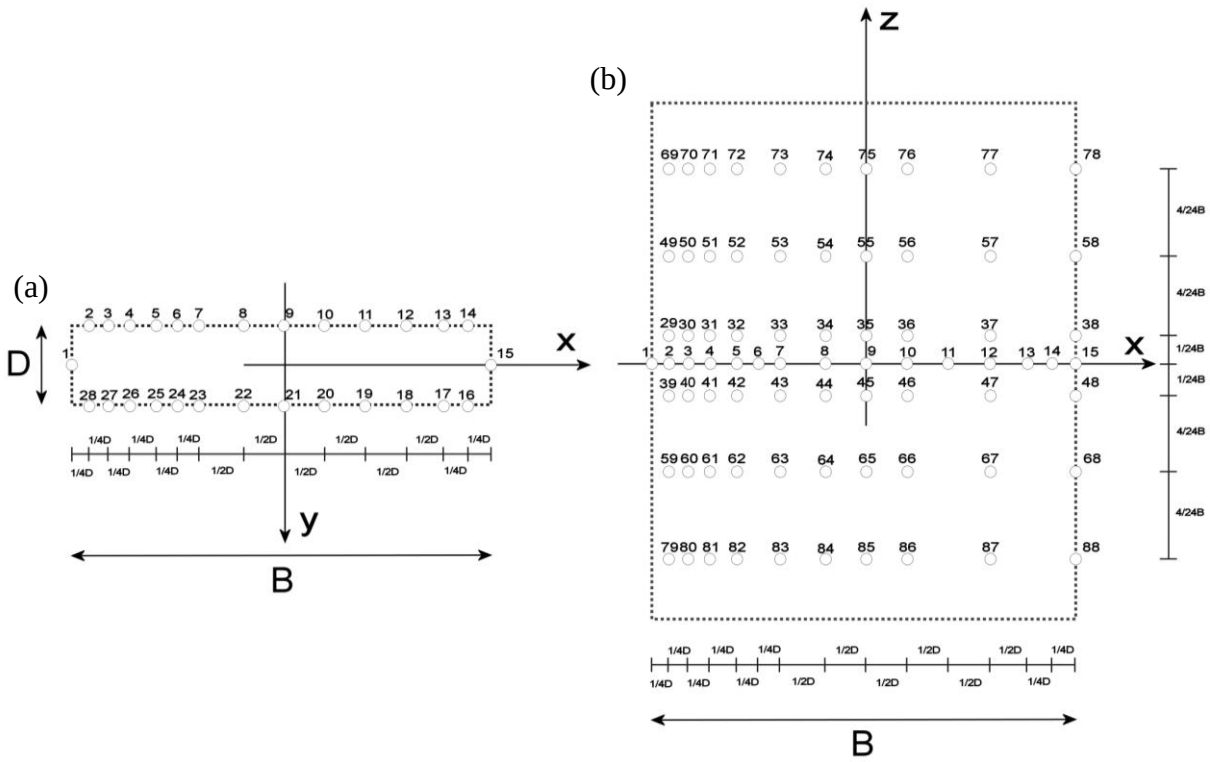

Figure 2. Pressure taps applied on the model in the centre section (a) and on the top face at six sections outside the centre (b). Dimensions are provided as fraction of the model thickness D (0.1 m) and the model width B (0.5 m).

3 RESULTS AND DISCUSSION

3.1 *Preliminary analysis*

Before the actual test plan could be performed, the time-averaged symmetry of the flow and the stationarity of some statistical quantities needed to be verified. The mean pressure coefficient in the stagnation point (tap 1 in Figure 2) was 1.0. Stationarity of the mean value, standard deviation, maximum and minimum pressure coefficient and the frequency content was investigated with a method described by Bruno et al (2010). Mean and standard deviation pressure coefficient were determined for increasing size of a non-dimensional sampling window $T_n = T_{n-1}+50$, in which $T_1 = 50$. Maximum and minimum value and frequency content were determined by averaging these characteristics, determined in each sampling window, over the sampling windows T_1 to T_n. The residual for the generic variable φ is determined at the n^{th} sampling window as $\varphi_{res} = |(\varphi_n-\varphi_{n-1})/\varphi_n|\cdot 100$. Figure 3 shows the convergence for the mean, standard deviation and peak pressure coefficients and frequency content. To avoid a residual larger than 5% a sampling extent $T_n \geq 400$ is needed. The sampling time of 120 s (tU/D = 9000) is more than sufficient to meet this requirement.

The initial measurement (M1) resulted in mean pressure coefficient distributions such as illustrated in Figure 4(a). The illustrated pressure coefficients were determined at the central section at zero degree angle of incidence. A deviation between the mean pressure distributions can be observed with a maximum difference of $\Delta C_{p,mean} = 0.12$ (13.6%) at $x/D = 2$. The standard deviation pressure coefficient distribution, illustrated in Figure 4(b), shows a maximum difference of 0.0193 at the same location as the mean. At the depth-wise position $x/D = 4$, defined by the BARC specifications for the check on local 2D features (pressure taps 12, 18, 37, 47, 57, 67, 77 and 87), $C_{p,mean}$ varies between -0.40 and -0.47 and $C_{p,std}$ varies between 0.22 and 0.24. Saathoff and Melbourne (1989) describe a difference in mean pressure distribution of 2% (after adjustment of the alignment). Hillier and Cherry (1981) obtained a $\Delta C_{p,mean}$ of 0.015 with the use of a trailing edge flap. Since these differences in mean pressure are much smaller than the values observed in this study, we decided to investigate the cause for this difference.

We considered six error sources responsible for the difference observed between both sides:

1. A disturbance in the oncoming flow
2. A misalignment between model and oncoming flow, caused by
    a. a misalignment of the model;
    b. an asymmetry in the flow;
3. Model inaccuracies
    a. Corner insert elements
    b. Pressure taps
    c. Quality of the rectangular shape of the model

3.2 *Disturbance in the oncoming flow*

The most significant source for disturbances in the flow was the pitot-static tube which was placed upstream of the model. This disturbance could be the reason for a local increase in turbulence intensity and influence the mean pressure distribution. However, this increased turbulence intensity should not only affect the mean pressure distribution, but also influence the standard deviation pressures. Furthermore, the oncoming flow measurements were performed with the pitot-static tube in the wind tunnel. Because no unexpected deviations were observed in longitudinal velocity or turbulence intensity in the region behind the pitot-static tube, the mean pressure difference could not have been caused by this disturbance in the flow.

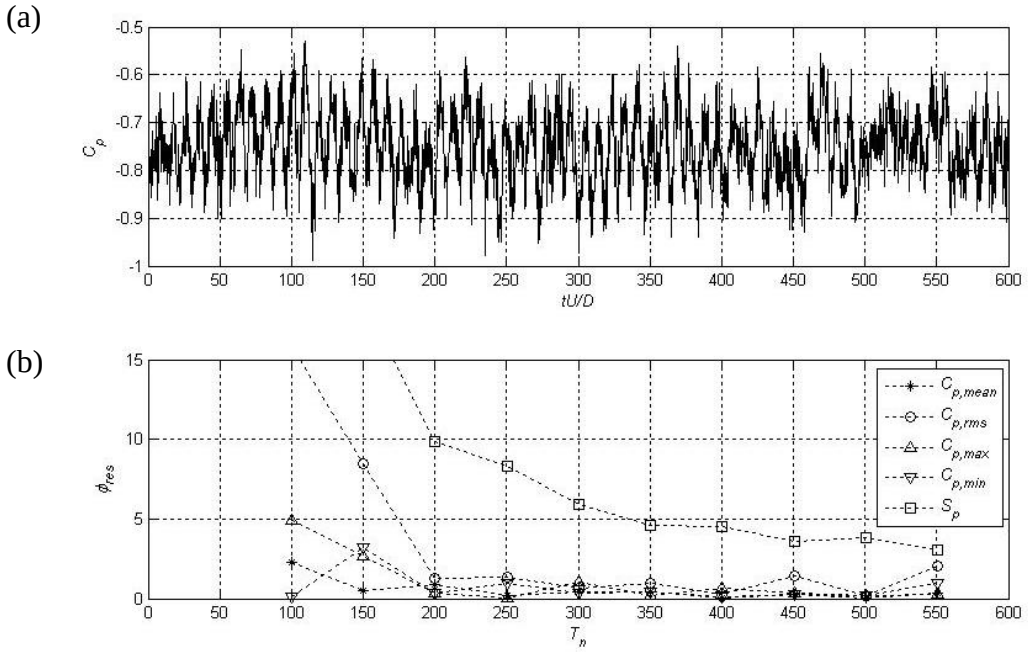

Figure 3. Time history of the pressure coefficient at pressure tap 5 (a) and the convergence of the characteristic values for mean, standard deviation, maximum, minimum and frequency content (b).

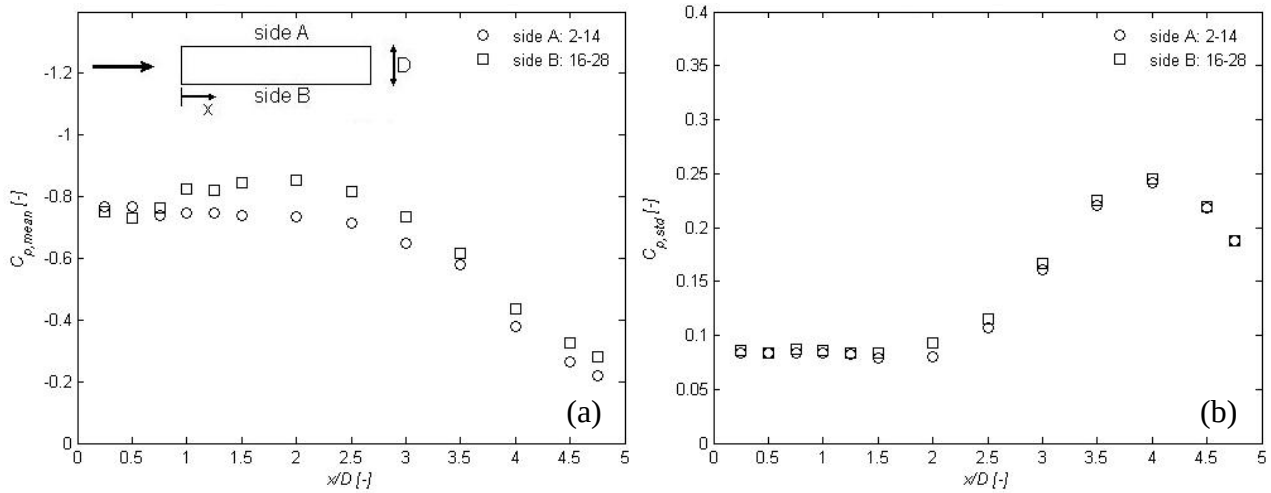

Figure 4. Mean (a) and standard deviation (b) pressure coefficient at the centre of the model. The pressure coefficient distributions on both sides of the model are shown to determine the symmetry of the distribution.

3.3 *Misalignment between model and oncoming flow*

The difference in mean pressure coefficient distribution, illustrated in Figure 4(a), could indicate side A is directed towards the oncoming flow. To investigate this possible misalignment of the model with the oncoming flow, measurements (M2 and M3) were performed at $\theta = -0.2^o$ and $\theta = -0.4^o$. Figure 5(a) and (b) illustrate the difference in mean and standard deviation pressure coefficient at these angles of incidence. The smallest differences in mean pressures are encountered at $\theta = -0.4^o$. However, the differences in standard deviation near the trailing at this angle of incidence indicate overcompensation of the misalignment. The difficulty to determine a clear zero degree angle of incidence, due to the large differences observed for all three measurements, are a sign that misalignment between oncoming flow and model is not the main cause for the difference between both sides. Implementation of a realignment based on the measured pressure distributions is also questionable, as it draws a strong assumption on the time-averaged symmetry of the flow field. Therefore the original zero degree setting of the model was used in further measurements.

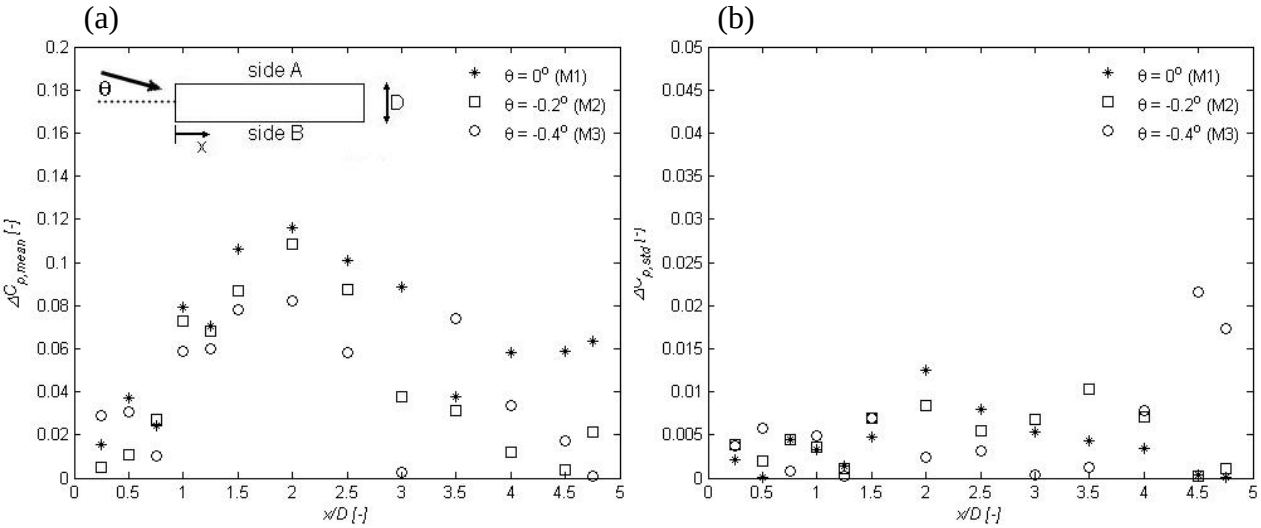

Figure 5. The absolute difference in mean (a) and standard deviation (b) pressure coefficient versus the model depth (*x/D*) at the central section. Differences for three angles of incidence are illustrated.

3.4 *Model inaccuracies*

The differences in mean pressure coefficients, shown in Figure 5(a), indicate that another effect is responsible for a local deviation in mean pressure coefficient. Between *x/D* = 1 and *x/D* = 3.5 the difference in mean pressure coefficient is larger than at the other depth wise positions. This local effect could be the result of a disturbance or asymmetry in the flow or a result of model inaccuracies. A fourth test (M4) was performed with the model rotated over 180º, to determine which of these influences is responsible. Figure 6(a) and (b) illustrate the mean pressure coefficient distributions for -0.2º and 180º angle of incidence. The angle of incidence of -0.2º was chosen to reduce the difference in the rear, which is mainly a result of misalignment, and give a clearer illustration for the following observation. The difference in mean pressure coefficient observed in Figure 5(a) between x/D = 0.75 and x/D = 3.5 is not present in Figure 5(b), instead a deviation is now observed between x/D = 2.5 and x/D = 4.25. The shift of the difference with 180º rotation of the model suggests it is a result of a model inaccuracy. Possible model inaccuracies which could cause this local difference are (1) the corner inserts used for the edge sharpness sensitivity study, (2) the pressure holes or (3) the shape of the model.

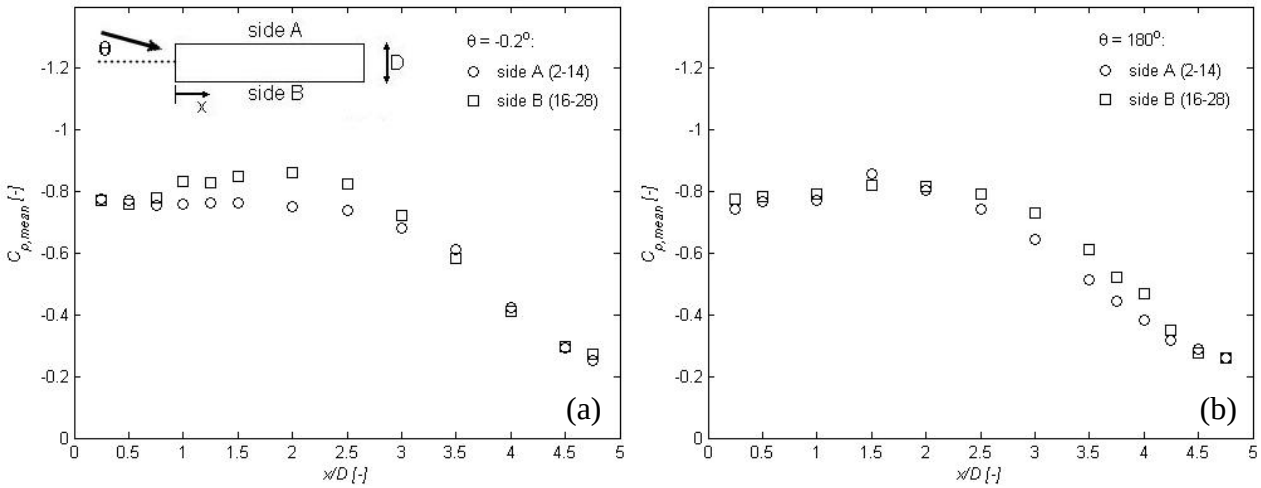

Figure 6. Mean pressure coefficient distributions at the central section of the model determined for: (a) -0.2º angle of incidence and (b) 180º angle of incidence.

Two more tests, M5 and M6, were performed to investigate the possible influence of the corner inserts and the influence of nearby pressure holes. For test M5, the inserts at the rear were swapped with the inserts in the front. No significant changes were observed on either mean or standard deviation pressure distribution in comparison with previous tests. To eliminate the possible influence of nearby pressure tap holes on the pressures measured at tap 2 to 14, the pressure tap rows 29-37, 39-47, 49-57 and 59-67 where closed off with tape. Again measurements indicated no significant differences between both sides.

No further measurements were performed to investigate the difference between both sides. To account for the uncertainty encountered in this experiment, mean and 95% confidence intervals of the pressure coefficient distributions over all span wise sections on the model were determined. Confidence intervals were only calculated at positions *x/D* at which six span wise pressure taps were located (see fFgure 2).

3.5 *Comparison with literature*

Figure 7(a) and (b) show the average values and 95% confidence intervals for the mean and standard deviation pressure coefficient distribution. Also illustrated are the experimental results of Hillier and Cherry (1981), Kiya and Sasaki (1983) and Saathoff and Melbourne (1989) for long flat plates and results obtained by Bruno et al (2010) obtained with an LES simulation on the BARC model (5:1 rectangular plate). The average of the mean pressure distribution over all sections [see Figure 7(a)] shows a good comparison with the results obtained by Hillier and Cherry (1981) and Saathoff and Melbourne (1989). Their results fit within the 95% confidence intervals determined in these measurements.

Figure 7(b) illustrates the average standard deviation pressure distribution and the 95% confidence intervals. The difference with the results found by Hillier and Cherry (1981) and Saathoff and Melbourne (1989) are a result of the larger B/D ratio applied in these studies (36 and 25 respectively). For these ratios, the fluctuations are only caused by the separation and reattachment of the flow. For ratios smaller than six, vortex shedding at the trailing edge interacts with leading edge separation, causing an increase in pressure fluctuations. A similar trend in standard deviation pressure coefficients was found by Bruno et al (2010).

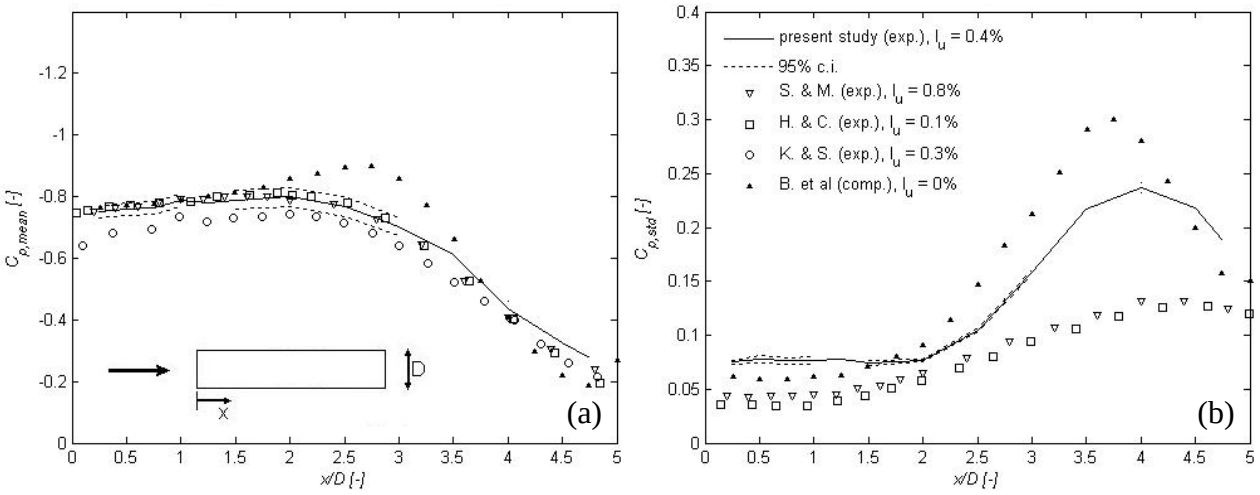

Figure 7. The average of the mean (a) and standard deviation (b) pressure coefficient distributions determined on the BARC model. At depth wise location x/D where there are 6 span wise pressure taps, 95% confidence intervals have been specified. Both Figure present results from literature: S. & M. (Saathoff and Melbourne, 1989), H. & C. (Hillier and Cherry, 1981), K. & S. (Kiya and Sasaki, 1983) and B. et al (Bruno et al, 2010).

4 CONCLUSION AND RECOMMENDATIONS

An experimental study on the pressures measured on a 5:1 rectangular cylinder has been presented in this paper. During the preliminary measurements to investigate the stationarity and symmetry of the flow and pressure distribution, a difference in mean pressure distribution between both sides of the model was encountered. The significance of the difference in comparison with differences mentioned in literature demanded a detailed investigation. Three possible causes (a disturbance in the flow, misalignment between model and flow, and model inaccuracies) were studied. Based on the performed investigation, the difference appears to be a result of an inaccuracy in model shape. Future measurements on all three velocity components of the oncoming flow and sensitivity measurements on the mean pressure distribution to the model shape will be useful to assure this conclusion.

To account for the uncertainty encountered in this study, the average and 95% confidence intervals of the pressure coefficient distributions were determined over all span wise sections on the model. The mean pressure coefficient distribution, averaged over all span wise sections, shows good agreement with results obtained from literature. The standard deviation pressure coefficient distribution shows a similar trend; the experimental values from literature are lower, which is a result of the plate depth to thickness ratio and the related flow phenomena.

Although no measurements were performed on the edge sharpness, the decision to investigate the observed differences will be useful for the development of a Best Practice guideline for these type of studies. Issues encountered in this study which in our opinion should be addressed in a guideline are:

- For a detailed description of the oncoming flow, velocity components in all three directions should be measured to determine possible asymmetries in the flow field.
- How should the zero degree angle of incidence be determined (i.e. through alignment of the model with the wind tunnel or with the oncoming flow) and how should misalignment be dealt with?
- How should model inaccuracies be investigated and dealt with?
- What variation in statistical quantities is acceptable for this type of measurement?
- Are reliability intervals an appropriate method to deal with the uncertainty encountered in these experiments?

5 REFERENCES

Bartoli, G., Bruno, L., Buresti, G., Ricciardelli, F., Saltelli, M.V., Zasso, A., 2008. BARC overview document <http://www.aniv-iawe.org/barc>.

Bruno, L., Fransos, D., Coste, N., Bosco, A., 2010, 3D flow around a rectangular cylinder: A computational study, J. Wind Eng. Ind. Aerodyn. 98, 263-276.

Hillier, R., Cherry, N.J., 1981. The effects of turbulent boundary-layer structure, J. Wind Eng. Ind. Aerodyn. 8, 49-58.

Kiya, M. and Sasaki, K., 1983. Freestream turbulence effects on a separation bubble, J. Wind Eng. Ind. Aerodyn. 14, 375-386.

Kiya, M. and Sasaki, K., 1985. Structure of large-scale vortices and unsteady reverse flow in the reattaching zone of a turbulent separation bubble, J. Fluid Mech. 154, 463-491.

Robertson, J.M., Wedding, J.B., Peterka, J.A., Cermak, J.E., 1977. Wall pressures of separation – reattachment flow on a square prism in uniform flow, J. Wind Eng. Ind. Aerodyn. 2, 345-359.

Saathoff, P.J., Melbourne, W.H., 1989. The generation of peak pressures in separated/reattaching flows, J. Wind Eng. Ind. Aerodyn. 32, 121-134.

Surry, D., Djakovich, D., 1995. Fluctuating pressures on models of tall buildings, J. Wind Eng. Ind. Aerodyn. 58, 81-112.